# Single attosecond pulse and xuv supercontinuum in the high-order harmonic plateau

Zenghu Chang*
*Department of Physics, Kansas State University, Manhattan, Kansas 66506, USA*
(Received 24 October 2003; revised manuscript received 14 May 2004; published 4 October 2004)

It is proposed that single attosecond pulses be generated by gating high-order harmonic emission with fields whose ellipticity varies rapidly with time. The laser pulse with a time-dependent ellipticity is created from two 5-fs laser pulses centered at 750 nm and separated by 5 fs. One of the laser pulses is left-circularly polarized and the other is right-circularly polarized. Numerical simulations show that when neon atoms are driven by such laser pulses, the generated high-order harmonic spectrum in the 25th to the 85th orders are a supercontinuum that corresponds to single attosecond pulses. A simple analytical expression is derived for estimating the high-harmonic radiation time.

DOI: 10.1103/PhysRevA.70.043802 PACS number(s): 42.65.Ky, 42.65.Re

## I. INTRODUCTION

Attosecond pulses are important tools for studying and controlling the motion of electrons inside atoms [1–4]. Until now, high-order harmonic generation (HHG) has been the only method that has produced single attosecond pulses [5,6]. A typical high-order harmonic spectrum shows that with the increase of harmonic order, the signal intensities fall off drastically for the first few low orders, then the intensities remain almost constant for many orders that form a plateau and finally the intensity drops abruptly for the highest orders, which have named the cutoff [3]. The harmonic generation process can be described by a three-step semiclassical model [7,8], i.e., an electron first tunnels out of the Coulomb potential barrier suppressed by the field and moves away from the ion, then the freed electron is driven back and accelerated when the laser field direction is reversed, finally it recombines with the ion. During the last step, an attosecond pulse is emitted.

The recollision that generates the cutoff harmonics occurs every half of an optical cycle, which results in two attosecond pulses per laser period [9]. The number of recollisions double for the generation of plateau harmonics, because there are two energy-degenerate electron trajectories per one half of a laser cycle that correspond to two recollisions [10]. Consequently, up to four attosecond pulses can be produced per laser cycles. At the present time, the shortest intense laser pulse is $\sim 5$ fs and centered at 750 nm, which is about two laser periods long. When it excites atoms to generated high-order harmonics, roughly three to four attosecond pulses are produced in the plateau region of the spectrum. The interference of the attosecond pulses produces discrete and well-resolved harmonic peaks [11,12]. Single attosecond pulses have been produced at the cutoff region only, i.e., in the laser cycle near the peak of the laser pulse. There are drawbacks to producing single attosecond pulses at the cutoff. The harmonic intensity there is lower than that in the plateau region. Furthermore, one needs to change the laser intensity and gas parameters to produce attosecond pulses at different wavelengths.

Harmonic generation driven by circularly or elliptically polarized laser pulses is much less efficient than that from a linearly polarized laser field [13,14]. In a circular laser field, the electron misses the ion when it returns. Since the high harmonic yield is sensitive to ellipticity of the laser field, it was proposed almost ten years ago that single attosecond pulses could be produced by laser pulses with a time-dependent ellipticity [15]. When the ellipticity varied from circular to linear, and then back to circular inside a laser pulse envelope, only the linearly polarized portion produced harmonics. In other words, the harmonic generation process is gated by the polarization of the laser pulse. It was proposed that the pulses with a time-dependent ellipticity could be formed by combining a left-circular pulse and a right-circular pulse with a certain delay [16]. The scheme is easier to implement than the superposition of two pulses with different center wavelengths as proposed in [15]. In [16], simulations were done for the superposition of two 20-fs circular laser pulses. Single attosecond pulse generation was predicted by selecting harmonics spatially. The proposed spatial filtering scheme is hard to realize experimentally.

In this paper, we propose to create the laser field whose ellipticity varies with time with two *few-cycle* circular pulses. By doing so, the polarization gating time is so short that single attosecond pulses can be generated *without spatial filtering*. The proposed method can be tested by using sub-10fs laser pulses from a hollow-core fiber/chirped mirror compressor. The paper is organized as follows: In Sec. II, we present a simple analytical expression for harmonic generation with pulses whose ellipticity varies with time. In Sec. III, the numerical simulation method is described. In Sec. IV, the simulation results for attosecond pulse generation with pulses whose ellipticity varies with time are presented. Finally, we discuss the results in Sec. V.

## II. ANALYSIS OF HHG WITH PULSES WITH A TIME-DEPENDENT ELLIPTICITY

The pulse with a time-dependent ellipticity is generated by the superposition of a left and a right-circularly polarized Gaussian pulse as proposed in [16]. The peak field amplitude $E_0$, carrier frequency $\omega$, pulse duration $\tau_p$ and carrier-envelope phase $\phi$ are the same for the two pulses. The delay

*Electronic address: chang@phys.ksu.edu

 

between them is $T_d$, which is an integral number, $n$, of optical periods. The electric fields of the left and right circularly polarized pulses propagating in the $z$ direction are

$$\vec{E}_l(t) = E_0 e^{-2\ \ln(2)((t-T_d/2)/\tau_p)^2}[\hat{x}\cos(\omega t+\phi)+\hat{y}\sin(\omega t+\phi)] \times(-1)^n, \quad (1)$$

$$\vec{E}_r(t) = E_0 e^{-2\ \ln(2)((t+T_d/2)/\tau_p)^2}[\hat{x}\cos(\omega t+\phi)-\hat{y}\sin(\omega t+\phi)] \times(-1)^n, \quad (2)$$

where $\hat{x}$ and $\hat{y}$ are unit vectors in the $x$ and $y$ directions, respectively.

The electric field of the combined pulse is

$$\vec{E}(t) = E_0\{\hat{x}[e^{-2\ \ln(2)((t-T_d/2)/\tau_p)^2}+e^{-2\ \ln(2)((t+T_d/2)/\tau_p)^2}] \times\cos(\omega t+\phi)+\hat{y}[e^{-2\ \ln(2)[(t-T_d/2)/\tau_p]^2} - e^{-2\ \ln(2)[(t+T_d/2)/\tau_p]^2}]\sin(\omega t+\phi)\}(-1)^n, \quad (3)$$

and the time-dependent ellipticity of the combined pulse is

$$\xi(t) = \frac{\left|e^{-2\ \ln(2)((t-T_d/2)/\tau_p)^2} - e^{-2\ \ln(2)((t+T_d/2)/\tau_p)^2}\right|}{e^{-2\ \ln(2)((t-T_d/2)/\tau_p)^2} + e^{-2\ \ln(2)((t+T_d/2)/\tau_p)^2}} = \frac{\left|1-e^{-4\ \ln(2)(T_d/\tau_p{}^2)t}\right|}{1+e^{-4\ \ln(2)(T_d/\tau_p{}^2)t}}. \quad (4)$$

Figure 1 shows the calculated ellipticity of the combined pulse using Eq. (4) when $T_d=\tau_p$. The ellipticity decreases linearly with $|t|$ in the center portion. $\xi=0$ at $t=0$, i.e., the light is linearly polarized. For harmonic order higher than the 21st, the harmonic signal drops by more than an order of magnitude when the ellipticity increases from 0 to 0.2 [13,14]. Therefore, we are interested only in the temporal range where the field is almost linearly polarized, i.e., $4\ \ln(2)(T_d/\tau_p^2)t \ll 1$, which yields

$$\xi(t) \approx \left|2\ \ln(2)\frac{T_d}{\tau_p^2}t\right|. \quad (5)$$

The linearity of Eq. (5) is also shown in Fig. 1. Clearly it is a good approximation of Eq. (4) for small $t$. The time interval, wherein the ellipticity is less than a certain value $\xi$, is thus

$$\delta t = \frac{1}{\ln(2)}\xi\frac{\tau_p^2}{T_d}. \quad (6)$$

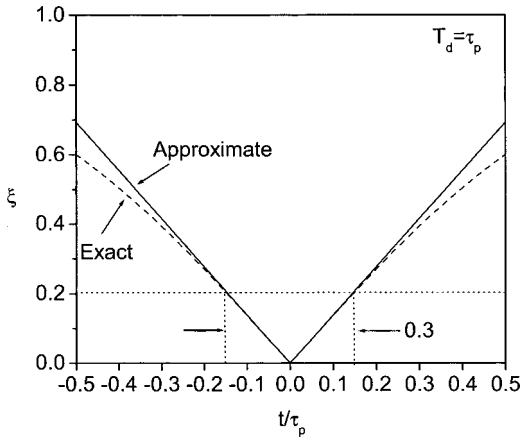


FIG. 1. The time-dependent ellipticity of the laser pulse formed by the combination of a left-hand circularly polarized pulse and a right-hand circularly polarized pulse. The pulse duration for each pulses is $\tau_p$ and the delay between them is $T_d$.

It suggests that there are two ways to reduce the high harmonic radiation time. One is to use shorter pulses and the other is to increase the delay between the pulses. The former is more effective because the radiation time depends on the square of the pulse duration. In other words, the shortest available laser pulses should be used. The latter approach is at the cost of losing laser field strength, which needs to be considered when the pulse energy available is limited as in the case when the pulses are produced from a hollow-core fiber pulse compressor. The amplitude of the linear field for a given delay and pulse duration can be calculated from Eq. (3) at $t=0$,

$$E(0) = 2E_0 e^{[-\ln(2)/2](T_d/\tau_p)^2}. \quad (7)$$

The field is significantly lower than the peak field of each pulse, $E_0$, for $T_d \gg \tau_p$. A good compromise is to choose $T_d=\tau_p$, which gives $E(0)=\sqrt{2}E_0$. Then

$$\delta t_{\xi\leqslant 0.2} = 0.3\tau_p, \quad (8)$$

which is also shown in Fig. 1.

Equation (8) indicates that for high harmonic generation, the combination of two circular pulses is equivalent to the reduction of the duration of a linearly polarized pulse by more than a factor of three without significant loss of the laser field strength. For the 20-fs laser pulse duration simulated in [16], $\delta t|_{\xi\leqslant 0.2} \approx 6$ fs, which is more than one laser period of a Ti:sapphire laser ($\sim$2.5 fs), attosecond pulse train are generated in the plateau region. In this case, the authors of [16] proposed to extract single attosecond pulses by spatially filtering the harmonic beams with pinholes. We pro-

pose to generate single attosecond pulses by polarization gating with laser pulses shorter than 10 fs. As an example, the harmonic emission time $\delta t_{\xi \leqslant 0.2}=1.5$ fs for the laser pulses with $\tau_p=5$ fs and $T_d=5$ fs. In such a short interval, it is expected that only one attosecond pulse is produced in the plateau region of the spectrum. Since spatial filtering is not necessary, the new scheme is easier to implement experimentally.

### III. THE SIMULATION METHOD

In high-order harmonic generation experiments, the measured harmonic signal is the coherent superposition of the radiation from all the atoms in the laser-atom interaction region. The circularly polarized laser pulses used to form the pulse with a time-dependent ellipticity were assumed to have a Gaussian shape with a carrier wavelength centered at 0.75 $\mu$m. In the next section, high harmonic generation from a neon gas target is simulated. First, the harmonic generation from the single atom driven by a pulse with time-dependent ellipticity is simulated using the Lewenstein model [17], then the macroscopic harmonic signal is calculated by solving a three dimensional wave equation for the harmonic field. The purpose of this work was to show the general nature of the polarization gating with a sub-10 fs laser pulse, not to simulate any particular experiments.

The Lewenstein model can be considered as the quantum expression of the three-step model [7,8], with which the dipole moment of an atom in the time domain, $\vec{r}(t)$, is calculated with the integral,

$$\vec{r}(t) = i\int_0^\infty d\tau\left(\frac{\pi}{\varepsilon + i\tau/2}\right)^{3/2} \vec{d}^*[\vec{p}_s(t,\tau) - \vec{A}(t)]a^*(t)e^{-iS(\vec{p}_s,t,\tau)} \times \vec{E}(t-\tau)\cdot\vec{d}[\vec{p}_s(t,\tau) - \vec{A}(t-\tau)]a(t-\tau) + \text{c.c.}, \quad (9)$$

where $\vec{E}(t)$ is the electric field of the laser pulse with a time-dependent ellipticity described by Eq. (3). $\vec{A}(t)$ is the vector potential. $\varepsilon$ is a small number, $\vec{p}_s(t,\tau)=\int_{t-\tau}^{t} dt''\vec{A}(t'')/\tau$ is the canonical momentum of the electron corresponding to a stationary phase. $S(\vec{p},t,t')$ is the quasiclassical action of the electron. $I_p=21.56$ eV is the ionization potential of the neon atom. $a(t)$ is the ground-state amplitude, which is calculated by the ADK theory [18,19]. The neon atom is chosen to avoid significant depletion of the ground state at the calculated intensity, $6\times10^{14}$ W/cm$^2$. Several experiments were done with neon gas at similar intensities and 5–7 fs linearly polarized pulses were used [11,12]. Finally $\vec{d}[\vec{p}_s-\vec{A}(t)]$ is the field-free dipole transition matrix element between the ground state and the continuum state,

$$\vec{d}(\vec{p}) = i\frac{2^{7/2}}{\pi}\alpha^{5/4}\frac{\vec{p}}{(\vec{p}^2+\alpha)^3}, \quad (10)$$

where $\alpha=2I_p$. Harmonic orders higher than the 21st are considered in this work. The photon energy of the 21st order is 34.72 eV, which is significantly larger than the ionization potential of the neon atom. The Keldysh parameter was $\gamma=\sqrt{I_p/2U_p}=0.59<1$ at the chosen intensity, where $U_p$ is the ponderomotive potential. The Lewenstein model is valid under these conditions.

The dipole moment along the $\hat{x}$ direction of the laser field, $x(t)$, is calculated by the integral,

$$x(t) = i\int_0^\infty d\tau\left(\frac{\pi}{\varepsilon + i\tau/2}\right)^{3/2} d_x^*[\vec{p}_s(t,\tau) - \vec{A}(t)]e^{-iS(\vec{p}_s,t,\tau)}\{E_x(t-\tau)\cdot d_x[\vec{p}_s(t,\tau) - \vec{A}(t-\tau)] + E_y(t-\tau)\cdot d_y[\vec{p}_s(t,\tau) - \vec{A}(t,\tau)]|a(t)|^2 + \text{c.c.}, \quad (11)$$

and the dipole moment along the $\hat{y}$ direction is calculated by

$$y(t) \approx i\int_0^\infty d\tau\left(\frac{\pi}{\varepsilon + i\tau/2}\right)^{3/2} d_y^*[\vec{p}_s(t,\tau) - \vec{A}(t)]e^{-iS(\vec{p}_s,t,\tau)} \times\{E_x(t-\tau)\cdot d_x[\vec{p}_s(t,\tau) - \vec{A}(t-\tau)] + E_y(t-\tau)\cdot d_y[\vec{p}_s(t,\tau) - \vec{A}(t-\tau)]\}|a(t)|^2 + \text{c.c.}, \quad (12)$$

where

$$d_x^*(\vec{p}_s(t,\tau) - \vec{A}(t)) = -i\frac{2^{7/2}}{\pi}\alpha^{5/4} \times \frac{p_{s,x}(t,\tau) - A_x(t)}{\{[p_{s,x}(t,\tau) - A_x(t)]^2 + [p_{s,y}(t,\tau) - A_y(t)]^2 + \alpha\}^3}, \quad (13)$$

$$d_y^*(\vec{p}_s(t,\tau) - \vec{A}(t)) = -i\frac{2^{7/2}}{\pi}\alpha^{5/4} \times \frac{p_{s,y}(t,\tau) - A_y(t)}{\{[p_{s,x}(t,\tau) - A_x(t)]^2 + [p_{s,y}(t,\tau) - A_y(t)]^2 + \alpha\}^3}. \quad (14)$$

The expressions for the matrix elements $d_x(\vec{p}_s(t,\tau)-\vec{A}(t-\tau))$ and $d_y(\vec{p}_s(t,\tau)-\vec{A}(t-\tau))$ are similar to Eqs. (13) and (14) except the vector potential is at the time $t-\tau$. The two components of the momenta are calculated by $p_{s,x}(t,\tau)=\int_{t-\tau}^{t} dt'' A_x(t'')/\tau$, and $p_{s,y}(t,\tau)=\int_{t-\tau}^{t} dt'' A_y(t'')/\tau$.

Finally, the action is calculated by

$$S(\vec{p}_s,t,\tau) = I_p\tau - \frac{1}{2}[p_{s,x}^2(t,\tau) + p_{s,y}^2(t,\tau)] + \frac{1}{2}\int_{t-\tau}^{t} dt''[A_x^2(t'') + A_y^2(t'')]. \quad (15)$$

Single atom calculations show that the amplitude of the harmonic spectrum amplitude along $\hat{y}$ is much smaller than that along $\hat{x}$, thus, only the latter is considered in this paper. The $\hat{y}$ component is negligible because the laser field is aligned to the $\hat{x}$ direction when it is almost linearly polarized.

The macroscopic harmonic signal from all the atoms in the target is calculated by solving the wave propagation

equation in the moving frame for the harmonic field, $E(\omega_H,r,z)$, in the frequency domain [11],

$$\nabla_\perp^2 E(\omega_H,r,z) - \frac{2i\omega_H}{c}\frac{\partial E(\omega_H,r,z)}{\partial z} = -\omega_H^2\mu_0 P_{nl}(\omega_H,r,z), \tag{16}$$

where $\omega_H$ is the frequency of the harmonic field, $r$ is the transverse coordinates, $z$ is the propagation coordinates in the moving frame that has the same value as in the laboratory frame, $c$ is the speed of light in vacuum, and $\mu_0$ is the permeability of free space. The nonlinear polarization $P_{nl}(\omega_H,r,z)\propto x(\omega_H,r,z)$, and $x(\omega_H,r,z)$ is dipole moment of an atom at $(r,z)$ that is the Fourier transform of the $x(t,r,z)$ calculated with Eq. (11) for that atom. This is called nonadiabatic approach [20,11].

The laser is a Gaussian beam propagating in the $z$ direction. Cylindrical symmetry with respect to the $z$ axis is assumed. The beam waist at the focus is $w_0=25$ $\mu$m, which gives a Rayleigh range $z_R=2.6$ mm. A 1 mm long gas target is centered at 2 mm after the laser focus. The atomic density of the target is assumed to be a constant. Equation (16) is solved numerically for each frequency in a spatial grid. The numbers of frequency is on the order on $10^{12}$. The numbers of grid point are 100 in the $r$ direction and are 400 in the $z$ direction. The single atom dipole moments at the grid points are calculated first and then are entered into Eq. (16) through the polarization $P_{nl}(\omega_H,r,z)$. Plasma effects are ignored in the simulation. The output spectrum is calculated by adding up the power spectrum at each transverse point at the exit of the target [11].

To obtain the harmonic pulse in the time domain, a square spectral window is applied to the harmonic spectrum at each transverse point at the exit of the target, and inverse Fourier transforms are performed to obtain the harmonic pulse for that point. The pulses of all the points are summed up to obtained the final pulse intensity. The narrowest window that supports harmonic pulses less than 1 fs is determined by the uncertainty principle. For square windows with width $\Delta\omega_h$,

$$\tau_h\frac{\Delta\omega_h}{2\pi}\approx 1, \tag{17}$$

where $\tau_h$ is the FWHM of the sinc function in the time domain. For $\tau_h=1$ fs, $\hbar\Delta\omega_h=4.14$ eV that is a little less than three times the photon energy ($\hbar\omega=1.65$ eV) of the driving laser. In our simulations, the width of the square window is $\Delta W=6\hbar\omega=9.9$ eV to reduce the effect of the window on the harmonic pulse duration.

## IV. HHG USING PULSES WITH A TIME-DEPENDENT ELLIPTICITY

For the comparison with harmonic generation driven by the laser pulse with a time dependent ellipticity, the harmonic spectrum is simulated for Ne atoms excited by a single, *linearly* polarized 5 fs pulse at $6\times10^{14}$ W/cm$^2$. In this case, the electric field of the pulse,

$$\vec{E}(t) = \hat{x}E_0 e^{-2\ \ln(2)(t/\tau_p)^2}\cos(\omega t+\phi). \tag{18}$$

The harmonic spectrum from a single atom is shown in Fig. 2(a), the carrier-envelope phase of the laser is assumed to be $\phi=0$ radian. The noiselike spectrum from a single atom is cleared up by the propagation that is calculated by the three dimensional wave equation. Well-resolved, odd harmonic orders are observed across the whole plateau, which was predicted previously in the calculation of [11] and was observed experimentally [11,12]. The two spectra are plotted in one figure to compare their structure, while their relative intensities are labeled arbitrarily.

Figure 2(b) shows the intensity normalized harmonic pulses corresponding to the selection of $\Delta W=6\hbar\omega$ around the 55th, and the 85th orders. The pulses centered at the 55th order represent the pulses in the plateau region, while the pulses centered at the 85th order are in the cutoff. For the former type of pulses, the single atom result is very different from the three dimensional one. It is well known that there are two dominant trajectories for the plateau harmonics, each trajectory produce an attosecond pulse. However, the long trajectory contribution is suppressed by the propagation because its phase depends strongly on the laser intensity [21,10]. That is why the number of attosecond pulses is less in the 3D case.

In the 3D case, the discrete orders in the plateau region correspond to attosecond pulse trains, i.e., three attosecond pulses separated by one half of a laser cycle. The number of pulses is determined by the number of recollisions between the field-liberated electron and the parent ion. The pulse duration of 5 fs (or two cycles) allows for three to four recollisions. The discrete order peaks in Fig. 2(a) were the results of the interference between the attosecond pulses. An analogy of this is the multislit interference in space. In order to generate a single attosecond pulse in the plateau, the duration of the driving pulse must be shorter than one optical cycle (2.5 fs). The generation of a single attosecond pulse with transient phase matching and rapid ionization using lasers pulse longer than the laser period has been investigated. Though it has yet to be demonstrated experimentally that the duration of the high-order harmonic pulse is indeed less than 1 fs [22].

There is only one attosecond pulse in the cutoff, which is the emission from a single recollision for the electron freed near the peak of the laser pulse. In fact, there is only one trajectory for the cutoff harmonics, thus the phase matching does not change the number of pulses in this case. Since the cutoff location is determined primarily by the laser intensity, i.e., $h\upsilon_{cutoff}=I_p+3U_p$, where $U_p$ is proportional to the laser intensity, one needs to change the laser intensity to tune the wavelength of the single attosecond pulses.

For 5 fs laser pulses, the harmonic spectra at the cutoff are sensitive to the carrier-envelope phase, which has been simulated before and is repeated by us. In Fig. 3(c), the spectrum correspond to a phase $\phi=0$ is compared with that of $\phi=\pi/2$. The resolvable harmonic peaks in the cutoff for $\phi=\pi/2$ is the result of the interference between two attosecond pulses. Recently, single attosecond pulses have been

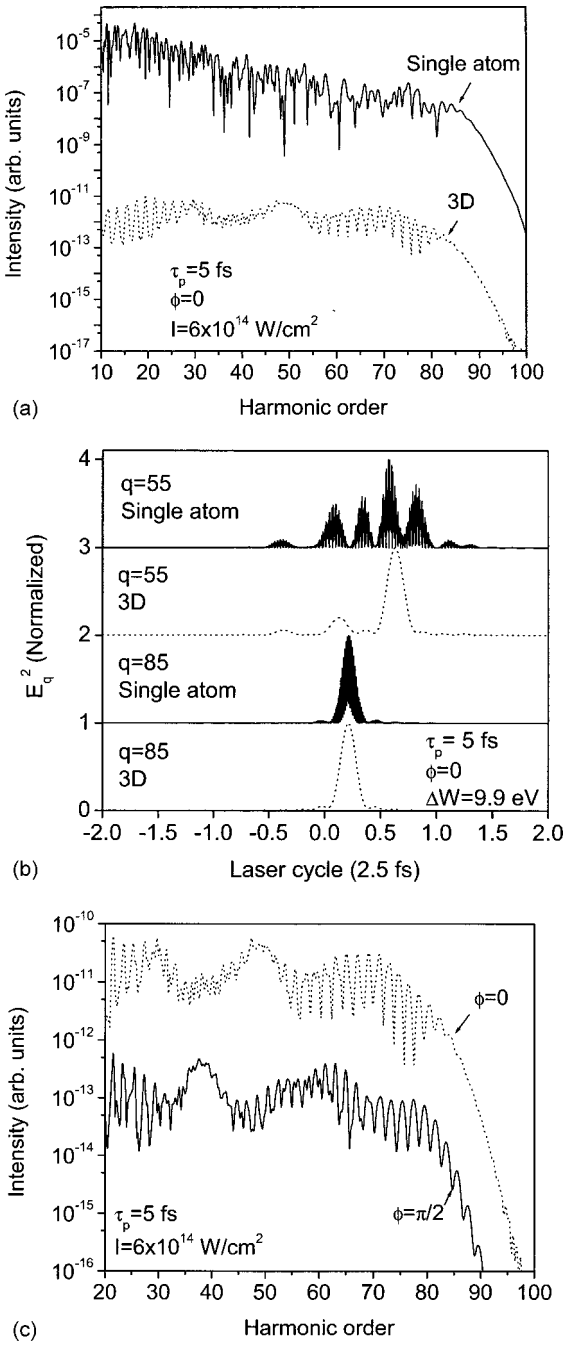


FIG. 2. (a) Comparison of the high-order harmonic spectrum from a single atom (solid line) with the result of the three-dimensional propagation (dot line). The gas target is neon gas driving by a linearly polarized laser pulse. The pulse duration is 5 fs centered at 0.75 $\mu$m. The peak intensity is $6\times10^{14}$ W/cm$^2$. The carrier-envelope phase of the laser pulse is 0 radian. (b) Effects of propagation on the high harmonic pulses at the plateau region (centers at $55\hbar\omega$) and at the cutoff region (centers at $85\hbar\omega$). The spectrum window is 9.9 eV. The solid line corresponds to the single atom calculation and the dot line is from the three-dimensional propagation simulation. (c) The effects of the carrier-envelope phase on the high harmonic spectra. The dot line and solid line correspond to $\phi=0$ and $\phi=\pi/2$, respectively.

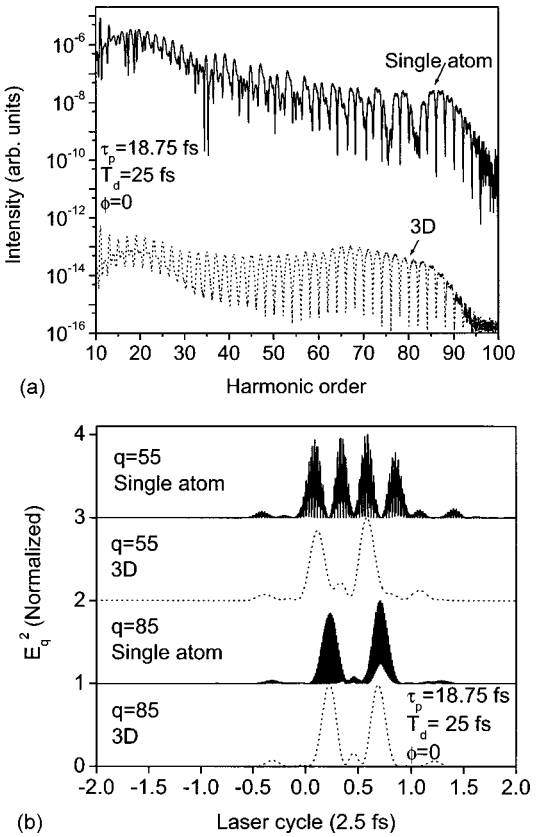


FIG. 3. (a) The high-order harmonic spectra from neon atoms driving by a laser pulse with a time-dependent ellipticity. The dot line corresponds to the single atom calculation and the solid line is from the three-dimensional propagation simulation. The laser pulse is formed by the combination of a left-hand circularly polarized pulse and a right-hand circularly polarized pulse. The pulse duration for both pulses is 18.75 fs and the delay between them is 25 fs. The peak intensity is $6\times10^{14}$ W/cm$^2$. The carrier-envelope phase of the laser pulse is 0 radian. (b) The high harmonic pulses centered at two different frequencies: $55\hbar\omega$ and $85\hbar\omega$. The spectrum window is 9.9 eV. The solid line correspond to the single atom calculation and the dot line is from the three-dimensional propagation simulation.

generated by using 5 fs pulses with the stabilized carrier-envelope phase.

In [16], simulations were done for the generation of high-order harmonics with pulses whose ellipticity varies with time. The pulse duration of each circular pulse was 7.5 cycles long and the delay between them was 10 cycles. The simulation is repeated here using the method described in Sec. III for laser pulses centered at 750 nm, which corresponded to two 18.75 fs circular pulses with a 25 fs delay. The carrier-envelope phases of the circular pulses are 0 radian. The peak intensity of the linear portion is $6\times10^{14}$ W/cm$^2$. The harmonic spectra from single atom and from 3D propagation are shown in Fig. 3(a). As in the case of harmonic generation using linearly polarized laser, the phase-matching clears up the spectrum. Well-resolved harmonic orders are seen over the whole spectrum of the 3D result, which indicates that two or more attosecond pulses are generated at the plateau and at the cutoff. The harmonic pulses for two center frequencies are shown in Fig. 3(b). For

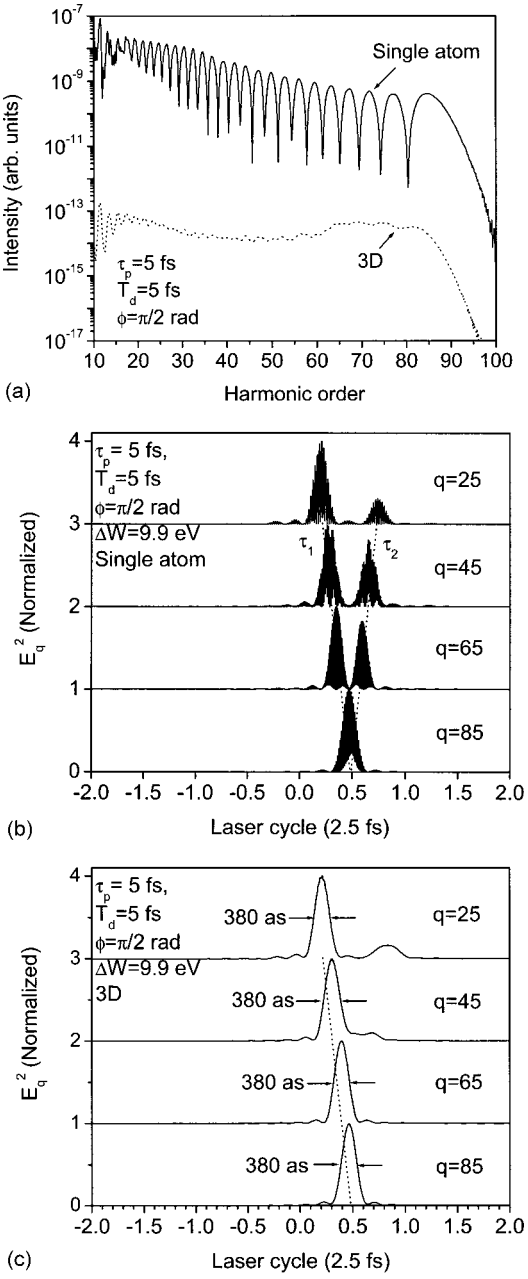


FIG. 4. (a) The high-order harmonic spectra from neon atoms driving by a laser pulse with a time-dependent ellipticity. The solid line corresponds to the single atom calculation and the dot line is from the three dimensional propagation simulation. The laser pulse is formed by the combination of a left-hand circularly polarized pulse and a right-hand circularly polarized pulse. The pulse duration for both pulses is 5 fs and the delay between them is 5 fs. The peak intensity is $6\times10^{14}$ W/cm$^2$ . The carrier-envelope phase of the laser pulse is $\phi=\pi/2$ radian. (b) The high harmonic pulses centered at four different frequencies: $25\hbar\omega$, $45\hbar\omega$, $65\hbar\omega$, and $85\hbar\omega$. The spectrum window is 9.9 eV. The results are obtained from the single atom calculation. (c) The attosecond pulses from the three-dimensional propagation simulation.

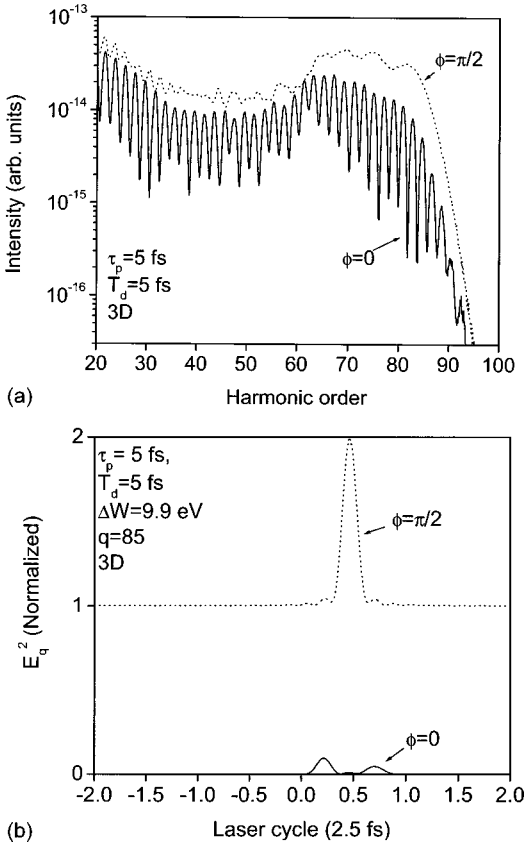


FIG. 5. (a) The high-order harmonic spectra from neon atoms driving by a laser pulse with a time-dependent ellipticity formed by the combination of a left-hand circularly polarized pulse and a right-hand circularly polarized pulse. The pulse duration for both pulses is 5 fs and the delay between them is 5 fs. The peak intensity is $6\times10^{14}$ W/cm$^2$. The dot line is when the carrier-envelope phase of the laser pulse is $\pi/2$ radian and the solid line is when the phase equals zero. (b) The high harmonic pulses centered at $85\hbar\omega$. The spectrum window is 9.9 eV. The upper curve (dot line) is when the carrier-envelope phase is $\pi/2$ radian. The lower curve (solid line) is for the phase equaling zero and its intensity is normalized to the upper one.

a single atom, four pulses are generated when their energies are centered at the 55th which is in the plateau region. However, two of them correspond to the long trajectories that are suppressed by the phase-matching. Consequently, only two attosecond pulses are left after the propagation as the 3D simulation shows. For the cutoff orders, both the single atom calculation and the 3D simulation show that two attosecond pulses are produced. This is because there is not one trajectory for the generation of cutoff harmonics. The authors of [16] suggested the extraction of a single attosecond pulse with pinholes.

The number of attosecond pulses in the plateau region shown in Fig. 3(b) is almost the same as that in Fig. 2(b), while a single 5 fs linearly polarized laser pulse is used. The results could be explained by the analysis in Sec. II. For the given pulse with a time-dependent ellipticity, the duration of the "linear" portion was $\delta t_{\xi<0.2}\approx0.3(18.75^2/25)\approx4.2$ fs, which was close to the duration of the linear pulse, 5 fs. In other words, for the generation of plateau harmonics, the

polarization gating is equivalent to reducing the linear pulse duration from 18.75 fs to 4.2 fs.

To avoid the technique difficulties of placing pinholes in the strong laser field as proposed in [16], i.e., the damage of the pinholes by the laser beam, we propose to use sub-10 fs ellipticity-dependent laser pulses for the polarization gating. Figure 4(a) showed the harmonic spectra without using any pinholes for the two circular pulses with 5 fs FWHM duration and with $\phi=\pi/2$ rad carrier-envelope phases. The delay between the two pulses is also 5 fs (two optical cycles). The peak intensity of the linear portion of the pulse with a time-dependent ellipticity is $6\times10^{14}$ W/cm$^2$. The 3D result shows that for orders above the 25th harmonic, the harmonic spectrum is a supercontinuum.

The phase-matching plays an important role in the generation of single attosecond pulses. In the plateau region, two attosecond pulses are emitted from a single atom. As shown in Fig. 2(b). The first one corresponds to the short trajectory (labeled by $\tau_1$) and the second one corresponds to the long trajectory (labeled by $\tau_2$). This is true for all of the four center frequencies. The modulation in the single atom spectrum is the results of the interference between the two pulses. The modulation period increase with the harmonic order because the pulse separation decreases. The spatial analogy is the Young's two-slit experiment with a variable split separation. After propagation, only the short trajectory survives, as shown in Fig. 4(c). The duration of the pulses are a little less than 400 attoseconds for the four different central frequencies located in a range from the deep plateau to the cutoff. The modulation depth of the 3D spectrum is much smaller than the single atom one because there is only one pulse left in the 3D case. The spatial analogy is the change of interference pattern when one of the slit is blocked in the Young's experiment. For the clearness of presentation, the pulse intensities are normalized in Figs. 4(b) and 4(c). It is noticed that the emission time also depends on the central frequency. For example, the attosecond pulse centered at the 85th order is delayed by $\sim$0.3 optical period as compared to the pulse centered at the 25th order. This is because the emission and recollision time are different for different harmonic orders.

The results show that when the circular pulses are 2 cycles long, it is not necessary to place pinholes to generate single attosecond pulses. The single attosecond pulse generation in the plateau can be understood by the analysis in Sec. II. As is shown there, for the given laser parameters, the "linear" portion in this case was $\delta t_{\xi<0.2}\approx1.5$ fs, less than one optical cycle. Two recollisions occur in such a short time interval, but the emission from one of them is eliminated by the phase matching.

Fig. 5(a) shows harmonic spectra obtained under the same conditions as Fig. 4(a) except for the carrier-envelope phase. In the figure, the dashed line corresponds to $\phi=\pi/2$, and the solid line is for $\phi=0$. In the former case, the plateau harmonics is a supercontinuum. For the latter pulses, however, harmonic peaks appear, indicating that more than one attosecond pulses is produced in the plateau region and in the cutoff. The attosecond pulses centered at the 85th harmonic is shown in Fig. 5(b). Indeed, there are two attosecond pulses for $\phi=0$ whose intensity is much lower than that of the single attosecond pulse when $\phi=\pi/2$. Therefore, the carrier-envelope phase significantly affects the attosecond pulse generation process. It is interesting that for generating single attosecond pulse the favorite carrier-envelope phase is $\phi=\pi/2$ in the case of polarization gating, while it is $\phi=0$ for using linearly polarized pulses. In order to produce single attosecond pulses from every laser shot, the carrier-envelope phase must be stabilized. The stabilization of the carrier-envelope phase has been demonstrated recently for intense sub-10 femtosecond laser pulses [12].

## V. CONCLUSIONS

It is shown analytically that the xuv pulse in the plateau harmonics generated using a driving pulse formed by a combination of a left-hand and a right-hand circular pulse with a pulse duration of $\tau_p$ is similar to using a linearly polarized pulse with a pulse duration of $0.3(\tau_p^2/T_d)$, where $T_d$ is the delay between the two pulses. Numerical simulations demonstrate that when $\tau_p=5$ fs, the harmonic spectrum using the pulse with a time-dependent ellipticity is a supercontinuum, which corresponds to single attosecond second pulses with a center wavelength at the plateau and in the cutoff. No harmonic selection with pinholes is necessary for such short driving laser pulses. For applications of attosecond pulses, the supercontiuum provides an easy way to change the wavelength of the attosecond pulse, which is important for time-resolved absorption spectroscopy [23].

## ACKNOWLEDGMENT

This work is supported by the Division of Chemical Sciences, Office of Basic Energy Sciences, US Department of Energy.

[1] T. Brabec and F. Krausz, Rev. Mod. Phys. **72**, 545 (2000).
[2] F. Krausz, Phys. World **14**, 41 (2001).
[3] P. Salieres, A. L'Huillier, Ph. Antoine, and M. Lewenstein, Adv. At., Mol., Opt. Phys. **41**, 83 (1999).
[4] M. Drescher, M. Hentschel, R. Kienberger, M. Uiberacker, V. Yakovlev, A. Scrinzi, Th. Westerwalbesloh, U. Kleineberg, U. Heinzmann, and F. Krausz, Nature (London) **419**, 803 (2002).
[5] M. Hentschel, R. Kienberger, Ch. Spielmann, G. A. Reider, N. Milosevic, T. Brabec, P. Corkum, U. Heinzmann, M. Drescher, and F. Krausz, Nature (London) **414**, 509 (2001).
[6] R. Kienberger, M. Hentschel, M. Uiberacker, Ch. Spielmann, M. Kitzler, A. Scrinzi, M. Weiland, Th. Westerwalbesloh, U. Kleineberg, U. Heinzmann, M. Drescher, and F. Krausz, Science **297**, 1144 (2002).
[7] P. B. Corkum, Phys. Rev. Lett. **71**, 1994 (1993).
[8] K. C. Kulander *et al.* in *Super-Intense Laser-Atom Physics*,

Vol. 316 of NATO Advanced Study Institute, Series B: Physics (Plenum, New York, 1993), p. 95 .

[9] P. M. Paul, E. S. Toma, P. Breger, G. Mullot, F. Auge, Ph. Balcou, H. G. Muller, and P. Agostini, Science **292**, 1689 (2001).

[10] P. Antoine, A. L'Huillier, and M. Lewenstein, Phys. Rev. Lett. **77**, 1234 (1996).

[11] E. Priori, G. Cerullo, M. Nisoli, S. Stagira, S. De Silvestri, P. Villoresi, L. Poletto, P. Ceccherini, C. Altucci, R. Bruzzese, and C. de Lisio, Phys. Rev. A **61**, 063801 (2000).

[12] A. Baltuska, Th. Udem, M. Uiberacker, M. Hentschel, E. Goulielmakis, Ch. Gohle, R. Holzwarth, V. S. Yakovlev, A. Scrinzi, T. W. Hansch, and F. Krausz, Nature (London) **421**, 611 (2003).

[13] P. Antoine, A. L'Huillier, M. Lewenstein, P. Salières, and B. Carre, Phys. Rev. A **53**, 1725 (1996).

[14] Bing Shan, Shambhu Ghimire, and Zenghu Chang, Phys. Rev. A **69**, 021404(R) (2004).

[15] P. B. Corkum, N. H. Burnett, and M. Y. Ivanov, Opt. Lett. **19**, 1870 (1994); M. Ivanov, P. B. Corkum, T. Zuo, and A. Bandrauk, Phys. Rev. Lett. **74**, 2933 (1995); P. Antoine, D. B. Milosevic, A. L'Huillier, M. B. Gaarde, P. Salières, and M. Lewenstein, Phys. Rev. A **54**, R1761 (1996).

[16] V. T. Platonenko and V. V. Strelkov, J. Opt. Soc. Am. B **16**, 435 (1999).

[17] M. Lewenstein, P. Balcou, M. Y. Ivanov, A. L'Huillier, and P. B. Corkum, Phys. Rev. A **49**, 2117 (1994).

[18] M. V. Ammosov, N. B. Delone, and V. P. Krainov, Adv. Eng. Software **91**, 2008 (1986) [Sov. Phys. JETP **64**, 1191 (1986)].

[19] Ilkov *et al.*, J. Phys. B **25**, 4005 (1992).

[20] P. Salières, P. Antoine, A. d. Bohan, and M. Lewenstein, Phys. Rev. Lett. **81**, 5544 (1998).

[21] M. Lewenstein, P. Salières, and A. L'Huillier, Phys. Rev. A **52**, 4747 (1995).

[22] A. Paul, R. A. Bartels, R. Tobey, H. Green, S. Weiman, I. P. Christov, M. M. Murnane, H. C. Kapteyn, and S. Backus, Nature (London) **421**, 51 (2003).

[23] S. L. Johnson, P. A. Heimann, A. M. Lindenberg, H. O. Jeschke, M. E. Garcia, Z. Chang, R. W. Lee, J. J. Rehr, and R. W. Falcone, Phys. Rev. Lett. **91**, 157403 (2003).